PLANETESIMAL FORMATION IN MAGNETOROTATIONALLY DEAD ZONES: CRITICAL DEPENDENCE ON THE NET VERTICAL MAGNETIC FLUX

Satoshi Okuzumi
Department of Physics, Nagoya University, Nagoya, Aichi 464-8602, Japan; okuzumi@nagoya-u.jp

AND

Shigenobu Hirose
Institute for Research on Earth Evolution, JAMSTEC, Yokohama, Kanagawa 236-0001, Japan
ApJL Accepted, May 30, 2012

ABSTRACT

Turbulence driven by magnetorotational instability (MRI) affects planetesimal formation by inducing diffusion and collisional fragmentation of dust particles. We examine conditions preferred for planetesimal formation in MRI-inactive "dead zones" using an analytic dead-zone model based on our recent resistive MHD simulations. We argue that successful planetesimal formation requires not only a sufficiently large dead zone (which can be produced by tiny dust grains) but also a sufficiently small net vertical magnetic flux (NVF). Although often ignored, the latter condition is indeed important since the NVF strength determines the saturation level of turbulence in MRI-active layers. We show that direct collisional formation of icy planetesimal across the fragmentation barrier is possible when the NVF strength is lower than 10 mG (for the minimum-mass solar nebula model). Formation of rocky planetesimals via the secular gravitational instability is also possible within a similar range of the NVF strength. Our results indicate that the fate of planet formation largely depends on how the NVF is radially transported in the initial disk formation and subsequent disk accretion processes.

Subject headings: dust, extinction — magnetohydrodynamics (MHD) — planets and satellites: formation — protoplanetary disks — turbulence

1. INTRODUCTION

Formation of kilometer-sized planetesimals is the initial step of planet formation in protoplanetary disks. Several mechanisms have been proposed for planetesimal formation, which include gravitational instability (GI) of dust subdisks (e.g., Goldreich & Ward 1973; Johansen et al. 2007; Youdin 2011) and direct coagulation (e.g., Weidenschilling & Cuzzi 1993; Okuzumi et al. 2012). However, the outcome of these processes strongly depends on the turbulent state of the gas disk. Turbulence is know to concentrate particles of particular sizes, which could assist their gravitational collapse (Cuzzi et al. 2001; Johansen et al. 2007). On the other hand, turbulence also stirs up dust subdisks and thereby stabilizes GI (Turner et al. 2010). In addition, the relative velocity induced by turbulence can lead to catastrophic disruption of large dust particles (Johansen et al. 2008).

The magnetorotational instability (MRI; Balbus & Hawley 1991) has been thought as the most plausible driving mechanism of protoplanetary disk turbulence. The activity of MRI largely depends on non-ideal MHD effects (e.g., Sano & Miyama 1999; Bai & Stone 2011; Wardle & Salmeron 2012). A high ohmic resistivity creates an MRI-inactive "dead zone" near the midplane (Gammie 1996), which reduces turbulence strength. Importantly, the size of the dead zone depends on the amount of tiny dust particles, because they effectively reduce the gas ionization degree and hence enhance the resistivity (Sano et al. 2000). Although the dead zone has often been invoked as a favorable site for planetesimal formation (e.g., Ciesla 2007; Bai & Stone 2010; Youdin 2011), self-consistent modeling of the MRI–dust co-evolution has not been done so far.

Another important, but much less appreciated factor is the *net vertical flux* (NVF) of the magnetic fields. The NVF indeed matters since it determines the saturation level of MRI-driven turbulence (e.g., Hawley et al. 1995; Suzuki et al. 2010). This is especially true when a large dead zone is present, for which case the vertically integrated accretion stress decreases with decreasing NVF (Gressel et al. 2012; Okuzumi & Hirose 2011, henceforth OH11).

In this Letter, we investigate possible pathways of planetesimal formation taking into account the dependence of MRI-driven turbulence strength on dust size distribution and NVF strength. In our previous paper (OH11), we systematically studied the saturated state of MRI-driven turbulence with local stratified, ohmic-resistive MHD simulations. We obtained an analytic prescription for the saturation level as a function of the ohmic diffusivity and NVF strength. Using this prescription together with ionization balance calculation including grain charging, we are able to determine turbulence strength consistently with the amount of tiny grains and NVF strength. We consider the formation of rocky and icy planetesimals independently, because icy particles have a high sticking efficiency compared to rocky particles (Chokshi et al. 1993; Gundlach et al. 2011). We test direct collisional formation of icy planetesimals outside the snow line, and rocky planetesimal formation via GI inside the snow line.

2. MODEL DESCRIPTION

We consider a protoplanetary disk around a solar mass star. We take the gas surface density Σ_g from the minimum-mass solar nebula (MMSN) model of Hayashi (1981). The gas temperature is taken from the passive, optically thick disk model of Chiang & Goldreich (1997). This model well approximates the gas temperature inside a dead zone, since MRI-driven heating occurs mainly at the upper boundary of the active layer where the optical depth is small (Hirose & Turner 2011). The assumed temperature gives a snow line at orbital radius $r \sim 1$ AU. The gas density ρ_g depends on the distance

z from the midplane as $\rho_g = (\Sigma_g/\sqrt{2\pi}h)\exp(-z^2/2h^2)$, where h is the gas scale height given as the sound speed c_s divided by the Keplerian frequency Ω. Because of gas pressure support, the gas disk rotates at a slightly sub-Keplerian velocity. This causes systematic radial drift of dust particles relative to the mean gas motion. The drift speed reaches the maximum $|v_{dr,\max}| \approx 30$ m s^{-1} when the stopping time t_s of the particle equals Ω^{-1} (Weidenschilling 1977). At $r \sim 1$–5 AU, the dimensionless stopping time $\Omega t_s = 1$ corresponds to particle radius $a \sim 1$ m.

We consider MRI-driven with a dead zone. The most important turbulent quantity for dust evolution is the random velocity of the gas since it determines the collision velocity and diffusion coefficient of dust particles. OH11 found that the gas velocity dispersion at the midplane, $\delta v_{g,\mathrm{mid}}$, is well approximated as

$$\delta v_{g,\mathrm{mid}} = \sqrt{0.78\alpha_{\mathrm{core}}}c_s, \qquad (1)$$

where α_{core} is the accretion stress integrated over low altitudes and normalized by $\Sigma_g c_s^2$. Equation (1) holds no matter if the midplane is magnetically dead, since hydrodynamical waves created in active layers propagate across dead zone boundaries. OH11 also found that α_{core} is determined by the dead zone size and NVF as

$$\alpha_{\mathrm{core}} = \frac{510}{\beta_{\mathrm{NVF,mid}}}\exp\left(-\frac{0.54h_{\mathrm{res}}}{h}\right) + 0.011\exp\left(-\frac{3.6h_\Lambda}{h}\right), \quad (2)$$

where $\beta_{\mathrm{NVF,mid}} = 8\pi\rho_{g,\mathrm{mid}}c_s^2/B_{\mathrm{NVF}}^2$ is the midplane plasma beta defined by the NVF strength B_{NVF}, and h_{res} and h_Λ are quantities that characterize the vertical extent of the dead zone. Precisely, h_{res} is the height below which the characteristic MRI wavelength $\lambda_{\mathrm{res}} = 2\pi\eta/v_{Az}$ in the resistive MHD limit exceeds h, whereas h_Λ is the height below which the ohmic Elsasser number $\Lambda = v_{Az}^2/\eta\Omega$ falls below unity, where $v_{Az} = B_{\mathrm{NVF}}/\sqrt{4\pi\rho_g}$ is the Alfvén speed defined by the NVF and η is the ohmic diffusivity. Linear stability analysis (Sano & Miyama 1999) shows that ohmic resistivity suppresses the most unstable MRI mode at $\Lambda \lesssim 1$ ($z \lesssim h_\Lambda$) but less unstable modes survive as long as $\lambda_{\mathrm{res}} \lesssim h$ ($z \gtrsim h_{\mathrm{res}}$). Thus, the region $h_{\mathrm{res}} < z < h_\Lambda$ can be interpreted as the transition layer between the active and dead zones. The active layer extends up to $z = h_{\mathrm{ideal}}$, above which MRI is stabilized because of a low local plasma beta (Sano & Miyama 1999; OH11). In the saturated state, h_{ideal} is approximately given by $h_{\mathrm{ideal}} = [2\ln(\beta_{\mathrm{NVF,mid}}/3000)]^{1/2}h$ according to the simulations of OH11.

For given $\delta v_{g,\mathrm{mid}}$, the gas random velocity δv_g at each height z is given as $\delta v_g = \exp(z^2/4h^2)\delta v_{g,\mathrm{mid}}$ (OH11). The vertical diffusion coefficient for dust is given by $D_z = D_{z0}/[1+(\Omega t_s)^2]$ (Youdin & Lithwick 2007), where

$$D_{z0} \approx \delta v_g^2/3\Omega \qquad (3)$$

is the vertical diffusion coefficient for passive ($\Omega t_s \ll 1$) contaminants (Fromang & Papaloizou 2006; OH11). Note that Equation (3) applies even in dead zones, which is consistent with the fact that hydrodynamical waves propagating from active layers have a finite correlation time $\sim \Omega^{-1}$ (Gressel et al. 2012). The turbulence-driven relative velocity Δv_t of dust particles is calculated from the prescription of Ormel & Cuzzi (2007) for Kolmogorov turbulence. In reality, a Kolmogorov energy cascade may not be established for waves in dead zones. However, the assumed Δv_t at least gives a reasonable
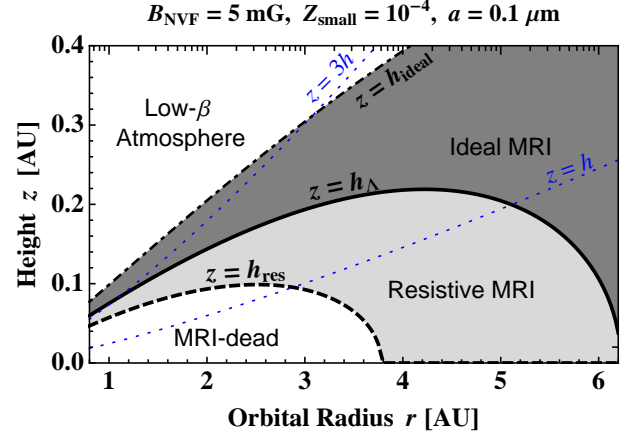
Figure 1. Example of the dead zone size. The dot-dashed curve shows $z = h_{\mathrm{ideal}}$ for $B_{\mathrm{NVF}} = 5$ mG, while the solid and dashed curves show $z = h_\Lambda$ and $z = h_{\mathrm{res}}$, respectively, for $B_{\mathrm{NVF}} = 5$ mG, $Z_{\mathrm{small}} = 10^{-4}$, and $a = 0.1\mu$m. For reference, $z = h$ and $3h$ are shown by the dotted curves.

estimate of the relative velocity for marginally or fully decoupled ($\Omega t_s \gtrsim 1$) particles since their relative velocity is determined by the largest-scale gas motion with correlation time $\sim \Omega^{-1}$ (see Ormel & Cuzzi 2007).

Equations (1) and (2) predict $\delta v_{g,\mathrm{mid}}$ as a function of h_{res}, h_Λ, and B_{NVF}. We calculate the critical heights by considering the ionization balance at each z taking into account grain charging. We use the analytic solution of the ionization balance equations derived by Okuzumi (2009), which gives the ionization degree for arbitrary dust size distribution. The ionizing sources we include are Galactic cosmic rays (Umebayashi & Nakano 2009), stellar X-rays (Igea & Glassgold 1999; Bai & Goodman 2009), stellar energetic protons (Turner & Drake 2009), and radionuclides (Umebayashi & Nakano 2009). Inclusion of cosmic and stellar protons gives the minimum estimate of the dead zone size since strong T-Tauri winds may shield these particles well above disk surfaces. From the ionization balance, we calculate the vertical profile of η (Blaes & Balbus 1994), and obtain h_{res} and h_Λ for given B_{NVF}. Figure 1 plots $z = h_{\mathrm{res}}$ and $z = h_\Lambda$ versus r for $B_{\mathrm{NVF}} = 5$ mG assuming that 0.1 μm sized grains are uniformly mixed in the gas with mass abundance $Z_{\mathrm{small}} \equiv \Sigma_{\mathrm{small}}/\Sigma_g = 10^{-4}$. Note that the dead zone size depends on B_{NVF}; the larger B_{NVF} is, the smaller h_{res} and h_Λ are.

3. ICY PLANETESIMAL FORMATION ACROSS THE FRAGMENTATION BARRIER

Planetesimal formation via direct coagulation is limited by the fact that marginally decoupled ($\Omega t_s \sim 1$, $a \sim 1$ m) dust aggregates experience high-speed collisions that can lead to catastrophic disruption (the so-called fragmentation barrier; Brauer et al. 2008). If the disk is laminar, the maximum collision velocity is determined by the differential radial drift velocity $\sim |v_{dr,\max}| \sim 30$ m s^{-1} (Brauer et al. 2008). Recent numerical collision experiments (Wada et al. 2009) show that aggregates made of submicron-sized icy grains stick at collision velocities up to ≈ 50 m s^{-1}, suggesting that icy planetesimal formation via direct coagulation is possible in laminar disks. However, if the disk has MRI-active layers, a random velocity of $\sim \delta v_{g,\mathrm{mid}}$ is added to the collision velocity for $\Omega t_s \sim 1$ aggregates (Ormel & Cuzzi 2007). The question is: can icy aggregates grow across the fragmentation barrier even if the MRI-driven turbulence enhances the collision velocity?

To get a feeling of how the fragmentation barrier depends on dust size distribution and NVF, we begin with a simple
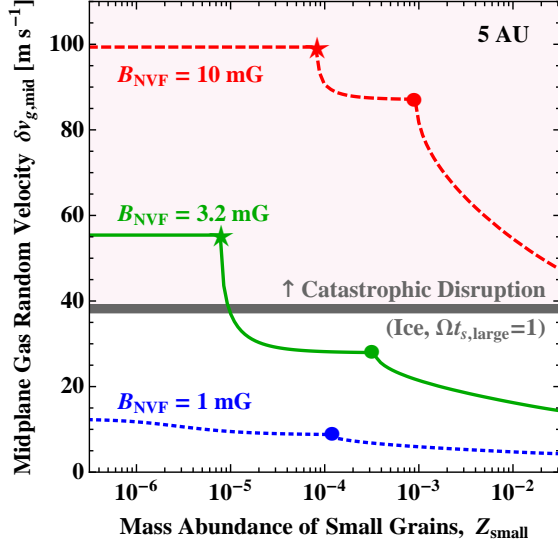
Figure 2. Midplane gas random velocity $\delta v_{g,\mathrm{mid}}$ at 5 AU vs. the mass abundance Z_{small} of small grains for different values of the NVF strength B_{NVF}. The filled circles and stars mark Z_{small} below which h_{res} and h_{Λ} vanish, respectively. Above the thick gray line, the total collision velocity for large ($\Omega t_{s,\mathrm{large}} \sim 1$) aggregates exceeds the catastrophic disruption threshold for ice (Wada et al. 2009).

two-population model in which large, marginally decoupled ($\Omega t_{s,\mathrm{large}} \sim 1$) aggregates coexist with 0.1 μm sized small grains. We calculate $\delta v_{g,\mathrm{mid}}$ assuming that only the small grains contribute to the ionization balance. The mass abundance Z_{small} of the small grains is taken as a free parameter. Figure 2 shows $\delta v_{g,\mathrm{mid}}$ as a function of Z_{small} for different values of B_{NVF}. For fixed B_{NVF}, $\delta v_{g,\mathrm{mid}}$ increases with decreasing Z_{small} because the dead zone is smaller when small grains are less abundant. The thick gray line shows $\delta v_{g,\mathrm{mid}} = 38$ m s^{-1}; above this line, the total collision velocity for two $\Omega t_s \sim 1$ aggregates, $\Delta v_{\mathrm{large}} \sim (\delta v_{g,\mathrm{mid}}^2 + v_{dr,\mathrm{max}}^2)^{1/2}$, exceeds the disruption velocity $v_{\mathrm{disr}} = 50$ m s^{-1} for icy aggregates (Wada et al. 2009). If $B_{\mathrm{NVF}} = 1.1$ mG, $\Delta v_{\mathrm{large}}$ falls below v_{disr} for all values of Z_{small}. The reason is two-fold. For such small B_{NVF}, a substantially large ($h_{\Lambda} \sim h$) dead zone is present even in the absence of small grains (note that h_{Λ} is larger when B_{NVF} is smaller). In addition, the small B_{NVF} leads to a low saturation level in the upper active layer, resulting in a low gas velocity dispersion (note that $\delta v_{g,\mathrm{mid}} \propto B_{\mathrm{NVF}}$ when $h_{\Lambda} \gg h/4$). However, if B_{NVF} goes up to 3.2 mG, $\Delta v_{\mathrm{large}}$ exceeds v_{disr} for $Z_{\mathrm{small}} \lesssim 10^{-5}$, for which the active layer reaches the midplane ($h_{\Lambda} = 0$). For $B_{\mathrm{NVF}} \gtrsim 10$ mG, $\Delta v_{\mathrm{large}}$ exceeds v_{disr} even if Z_{small} is as large as the interstellar value 10^{-2}.

For $B_{\mathrm{NVF}} \sim 3$ mG, large aggregates can grow across the fragmentation barrier only if small grains are sufficiently abundant. To show that it is indeed possible, we simulate the evolution of full dust size distribution at 5 AU using a coagulation–advection–diffusion equation (e.g., Ciesla 2007). In this simulation, we begin with 0.1 μm icy dust grains well mixed in the vertical direction, and follow the evolution of the vertical dust size distribution due to coagulation/fragmentation and vertical settling/diffusion. The collision velocity Δv of dust particles takes into account Brownian motion, systematic drift in the mean gas motion (Nakagawa et al. 1986), and turbulence-driven random motion (Ormel & Cuzzi 2007) that depends on δv_g. We take δv_g to be time-dependent, namely, to be consistent with the

dead zone size calculated from the full dust size distribution (Okuzumi 2009) at each time step. The total dust mass abundance $Z = \Sigma_d/\Sigma_g$ is taken to be 10^{-2}, and the loss of dust materials due to the radial drift is neglected. Indeed, coagulation proceeds faster than radial migration if the dust grows into highly porous aggregates (Okuzumi et al. 2012). However, in order to make our model as simple as possible, we neglect both porosity evolution and radial migration. The mass of an aggregate after collision is given by $m_t + s m_p$, where m_t and $m_p (< m_t)$ are the masses of the target and projectile, and $s (\leqslant 1)$ is the dimensionless sticking efficiency that depends on Δv. We assume $s = 1$ for $\Delta v < 10$ m s^{-1} and $s = 1 - \ln(\Delta v/10 \text{ m s}^{-1})/\ln 5$ for $\Delta v > 10$ m s^{-1} in accordance with the result of numerical collision experiments for icy aggregates (Wada et al. 2009). The target loses its mass ($s < 0$) when Δv is larger than the disruption threshold $v_{\mathrm{disr}} = 50$ m s^{-1}. The fragments (whose total mass is $(1-s)m_p$) are assumed to be in the form of 0.1 μm sized constituent grains. This assumption is quite simplistic, but still is reasonable as a first-order approximation since the total mass of fragments in aggregate–aggregate collision tends to be dominated by the smallest ones (Wurm et al. 2005; Wada et al. 2009).
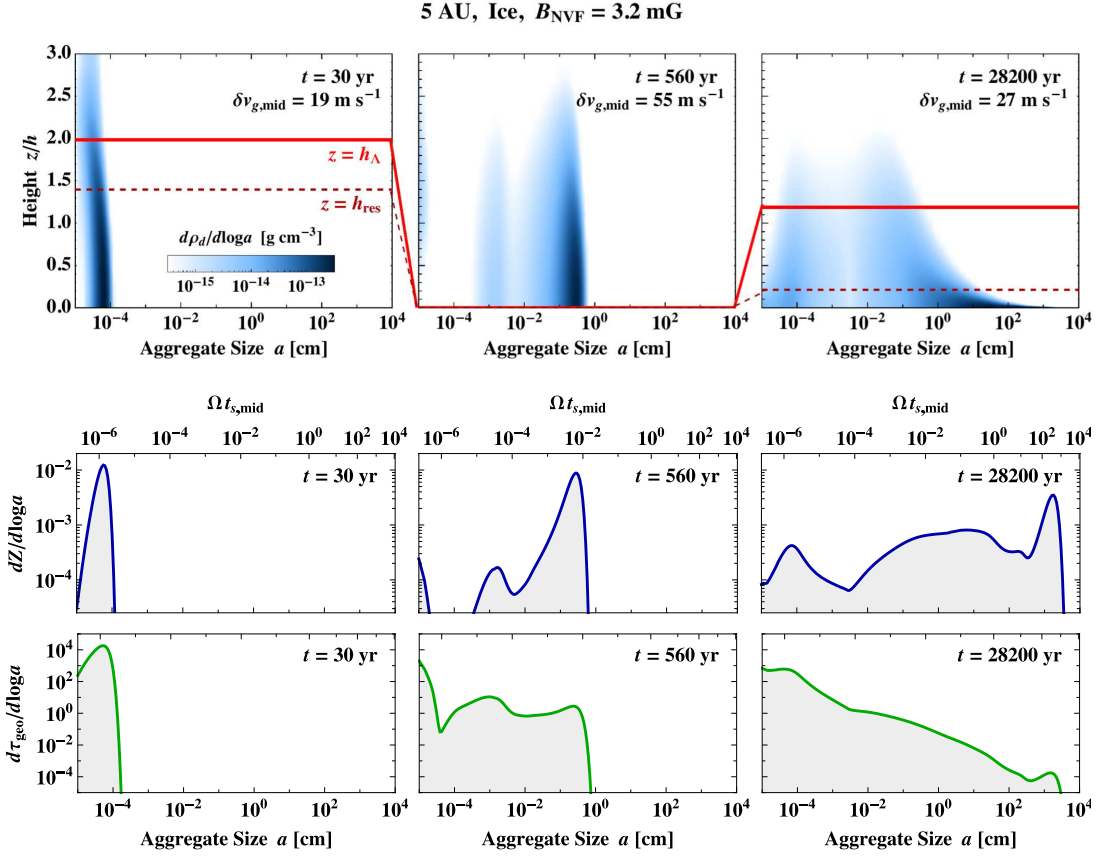
Figure 3 shows the simulation result for $B_{\mathrm{NVF}} = 3.2$ mG. The top panels display the vertical dust mass density ρ_d per unit logarithmic particle radius $\log a$ at different times t after the initial state. Initially, dust particles grow without catastrophic disruption because of low collision velocities. As the particles grow, disruption becomes more and more significant, because the collision velocity increases with increasing stopping time and because the dead zone shrinks with the depletion of small grains. The second effect becomes prominent when $t \approx 560$ yr, at which the dead zone disappears and consequently $\delta v_{g,\mathrm{mid}}$ reaches 55 m s^{-1}. However, the large amount of tiny grains produced by the catastrophic disruption are quickly diffused to high altitudes, reduce the ionization degree, and finally "revive" the dead zone. The revived dead zone suppresses $\delta v_{g,\mathrm{mid}}$ down to 27 m s^{-1}, which is low enough for larger aggregates to continue growing. In this way, larger aggregates grow beyond the meter-size fragmentation barrier.

The middle panels of Figure 3 plot the dust mass abundance Z per unit $\log a$, while the bottom panels show the vertical geometric optical depth τ_{geo} of dust per unit $\log a$. We see that the dust mass is dominated by large aggregates while the optical depth is dominated by small fragments. This indicates that small fragments carry a minor fraction of the total dust mass but still help the grow of larger aggregates by providing a large surface area needed to maintain a low enough ionization degree.

4. ROCKY PLANETESIMAL FORMATION VIA SECULAR GI

Coagulation of rocky aggregates is severely restricted by the fragmentation barrier since the disruption threshold is as low as 1–5 m s^{-1} (Wada et al. 2009; Güttler et al. 2010). Using that the radial drift speed $|v_{dr}|$ is approximated as $2|v_{dr,\mathrm{max}}|\Omega t_s$ for $\Omega t_s \ll 1$ (Weidenschilling 1977) and assuming that $v_{\mathrm{disr}} \approx 5$ m s^{-1} and $|v_{dr,\mathrm{max}}| \approx 30$ m s^{-1}, we find that $|v_{dr}|$ reaches v_{disr} when $\Omega t_s \approx 0.08$, which corresponds to $a \sim 10$ cm at ~ 1 AU. Hence, a simple coagulation scenario does not account for rocky planetesimal formation even without turbulence.

One mechanism that can lead to rocky planetesimal formation is the so-called secular GI (Youdin 2011). It is a gravitational collapse of dust materials driven by the combina-

5 AU, Ice, $B_{NVF} = 3.2$ mG

Figure 3. Result of a coagulation simulation for icy dust at 5 AU for $B_{NVF} = 3.2$ mG. The top density plots show the dust mass density ρ_d per unit logarithmic particle radius $\log a$ at different heights z and different times t. The solid and dashed lines in the top panels mark the dead zone critical heights $z = h_\Lambda$ and $z = h_{res}$, respectively. The middle and bottom panels show the mass abundance Z and geometric optical depth τ_{geo} of dust per unit $\log a$, respectively. Shown in the top of the middle panels is the dimensionless stopping time $\Omega t_{s,mid}$ of the dust particles at the midplane.

tion of self-gravity and gas friction. An important feature of the secular GI is that it works even if $\Omega t_s \ll 1$. Thus, the secular GI can allow gravitational collapse of dust particles whose growth is limited by the fragmentation barrier. Instead, the secular GI requires sufficiently weak radial dust diffusion in order for the particles to collapse faster than they drift inward. For $\Omega t_s \approx 0.1$, the radial diffusion coefficient D_r must be lower than $10^{-5}c_s h$ at the midplane (Youdin 2011; Takeuchi & Ida 2012).

To assess whether the secular GI operates for the fragmentation-limited aggregates, we estimate the MRI-driven diffusion coefficient assuming that the aggregates coexist with 0.1 μm sized fragments of mass abundance Z_{small}. We also assume that $D_r \approx D_z$, which is $\approx D_{z0}$ for $\Omega t_s \approx 0.1 \ll 1$ (see Equation (3)). Figure 4 shows the midplane radial diffusion coefficient $D_{r,mid}$ at 1 AU as a function of Z_{small} for different values of B_{NVF}. We find that $D_{r,mid}$ exceeds $10^{-5}c_s h$ for $B_{NVF} \gtrsim 10$ mG even if Z_{small} is as large as the interstellar value 10^{-2}. Thus, the secular GI of the fragmentation-limited aggregates requires $B_{NVF} \lesssim 10$ mG. This requirement is similar to to that for direct icy planetesimal formation shown in Section 3.

5. CONCLUSION AND DISCUSSION

We have investigated how planetesimal formation depends on the amount of tiny grains and the strength of the NVF. For MMSN disks, we have shown that the existence of a large dead zone *and* an NVF weaker than 10 mG is preferable for planetesimal formation via both direct coagulation and secu-
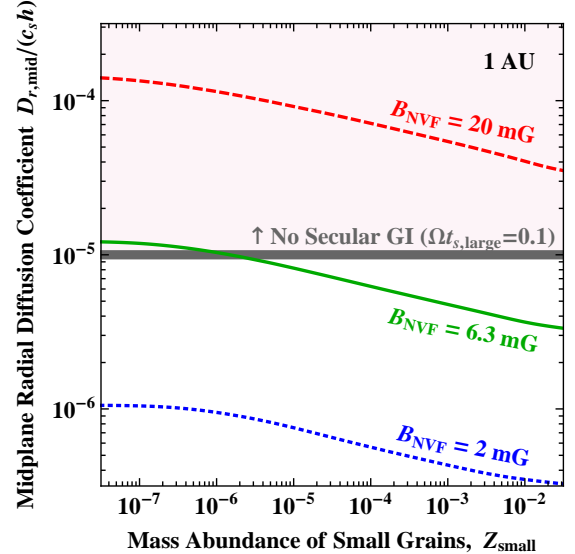
Figure 4. Midplane radial diffusion coefficient $D_{r,mid}$ at 1 AU vs. the mass abundance Z_{small} of small grains for different values of the NVF strength B_{NVF}. Below the thick gray line, the fragmentation-limited rocky aggregates ($\Omega t_{s,large} \approx 0.1$) experience secular gravitational collapse faster than they drift inward (Youdin 2011; Takeuchi & Ida 2012).

lar GI. The obtained criterion for the NVF depends on the disk surface density Σ_g, since $\delta v_{g,mid} \propto B_{NVF}/\sqrt{\Sigma_g}$ in the presence of a large dead zone (see Equations (1) and (2)). If Σ_g is 10 times larger than the MMSN value, then the upper limit on

B_{NVF} goes up to 30 mG.

We have neglected the effects of non-ohmic magnetic diffusivities. Ambipolar diffusion may stabilize MRI near the upper boundary of the active layer (Bai 2011). The effect of Hall diffusion is more uncertain; it can stabilize or destabilize MRI depending on the sign of NVF relative to the disk rotation axis (Wardle & Salmeron 2012). Inclusion of these effects may change our results quantitatively, but the general trend that a weak NVF is preferable may be unchanged.

Weak turbulence is also beneficial to the growth of solid objects larger than planetesimals. Density fluctuations in turbulence gravitationally interact with planetesimal-size objects and thereby enhance their collision velocity. If MRI is fully active, the resulting gravitational stirring likely causes catastrophic disruption of planetesimals (e.g., Ida et al. 2008; Nelson & Gressel 2010). However, Gressel et al. (2012) have recently shown that even weakly bound planetesimals are able to grow if a dead zone is present and if the NVF is weaker than 3 mG (assuming the MMSN surface density). Thus, a weak NVF and a wide dead zone are preferable for the growth of solid bodies up to protoplanets.

A realistic range of the NVF strength is poorly constrained by direct observations since the differential rotation of the disk can produce toroidal magnetic fields as strong as 0.1–1 G even inside the dead zone (Turner & Sano 2008). An important property of NVF is that the total NVF is a conserved quantity of a magnetized disk. Thus, the total NVF of a protoplanetary disk is directly determined by how the disk formed from weakly magnetized ($\sim 10\,\mu$G; Heiles & Crutcher 2005) molecular clouds. Nevertheless, what fraction of the magnetic flux is brought to the planet-forming inner disk region is not evident because non-ideal MHD processes also work during the disk formation (e.g., Machida et al. 2011). Furthermore, on longer timescales, the NVF may be radially transported due to inward mass accretion (Rothstein & Lovelace 2008) and/or outward macroscopic magnetic diffusion (Lubow et al. 1994) in the active layers. So far, the origin and global transport of NVF has not been paid attention in the context of planet(esimal) formation. We hope that this Letter will encourage further investigation on this issue.

REFERENCES

Bai, X.-N. 2011, ApJ, 739, 50
Bai, X.-N., & Goodman, J. 2009, ApJ, 701, 737
Bai, X.-N., & Stone, J. M. 2010, ApJ, 722, 1437
Bai, X.-N., & Stone, J. M. 2011, ApJ, 736, 144
Balbus, S. A., & Hawley, J. F. 1991, ApJ, 376, 214
Blaes, O. M., & Balbus, S. A. 1994, ApJ, 421, 163
Brauer, F., Dullemond, C. P., & Henning, Th. 2008, A&A, 480, 859
Chiang, E. I., & Goldreich, P. 1997, ApJ, 490, 368
Chokshi, A., Tielens, A. G. G. M., & Hollenbach, D. 1993, ApJ, 407, 806
Ciesla, F. J. 2007, ApJ, 654, L159
Cuzzi, J. N., Hogan, R. C., Paque, J. M., & Dobrovolskis, A. R. 2001, ApJ, 546, 496
Fromang, S., & Papaloizou, J. 2006, A&A, 452, 751
Gammie, C. F. 1996, ApJ, 457, 355
Goldreich, P., & Ward, W. R. 1973, ApJ, 183, 1051
Gressel, O., Nelson, R. P., & Turner, N. J. 2012, MNRAS, 422, 1240
Gundlach, B., Kilias, S., Beitz, E., & Blum, J. 2011, Icarus, 214, 717
Güttler, C., Blum, J., Zsom, A., Ormel, C. W., & Dullemond, C. P. 2010, A&A, 513, A56
Hawley, J. F., Gammie, C. F., & Balbus, S. A. 1995, ApJ, 440, 742
Hayashi, C. 1981, Prog. Theor. Phys. Suppl., 70, 35
Heiles, C., & Crutcher, R. 2005, in Cosmic Magnetic Fields, ed. R. Wielebinski & R. Beck (Lecture Notes in Physics, Vol. 664; Berlin: Springer), 137
Hirose, S., & Turner, N. J. 2011, ApJ, 732, L30
Ida, S., Guillot, T., & Morbidelli, A. 2008, ApJ, 686, 1292
Igea, J., & Glassgold, A. E. 1999, ApJ, 518, 848
Johansen, A., Brauer, F., Dullemond, C., Klahr, H., & Henning, T. 2008, A&A, 486, 597
Johansen, A., Oishi, J. S., Mac Low, M.-M., et al. 2007, Nature, 448, 1022
Lubow, S. H., Papaloizou, J. C. B., & Pringle, J. E. 1994, MNRAS, 267, 235
Machida, M. N., Inutsuka, S., & Matsumoto, T. 2011, PASJ, 63, 555
Nakagawa, Y., Sekiya, M., & Hayashi, C., 1986, Icarus, 67, 375
Nelson, R. P., & Gressel, O. 2010, MNRAS, 409, 639
Okuzumi, S. 2009, ApJ, 698, 1122
Okuzumi, S., & Hirose, S. 2011, ApJ, 742, 65 (OH11)
Okuzumi, S., Tanaka, H., Kobayashi, H., & Wada, K. 2012, ApJ, in press (arXiv:1204.5035)
Ormel, C. W., & Cuzzi, J. N. 2007, A&A, 466, 413
Rothstein, D. M., & Lovelace, R. V. E. 2008, ApJ, 677, 1221
Sano, T., & Miyama, S. M. 1999, ApJ, 515, 776
Sano, T., Miyama, S. M., Umebayashi, T., & Nakano, T. 2000, ApJ, 543, 486
Suzuki, T. K., Muto, T., & Inutsuka, S. 2010, ApJ, 718, 1289
Takeuchi, T., & Ida, S. 2012, ApJ, 749, 89
Turner, N. J., Carballido, A., & Sano, T. 2010, ApJ, 708, 188
Turner, N. J., & Drake, J. F. 2009, ApJ, 703, 2152
Turner, N. J., & Sano, T. 2008, ApJ, 679, L131
Umebayashi, T., & Nakano, T. 2009, ApJ, 690, 69
Wada, K., Tanaka, H., Suyama, T., Kimura, H., & Yamamoto, T. 2009, ApJ, 702, 1490
Wardle, M., & Salmeron, R. 2012, MNRAS, in press
Weidenschilling, S. J. 1977, MNRAS, 180, 57
Weidenschilling, S. J., & Cuzzi, J. N. 1993, in Protostars and Planets III, ed. E. H. Levy & J. I. Lunine (Tucson, AZ: Univ. Arizona Press), 1031
Wurm, G., Paraskov, G., & Krauss, O. 2005, Icarus, 178, 253
Youdin, A. N. 2011, ApJ, 731, 99
Youdin, A. N., & Lithwick, Y. 2007, Icarus, 192, 588